

# Vector Analysis of the Space-Charge Field in Nonconventionally Biased Photorefractive Crystals

C. Crognale, *Member, IEEE*, and L. Rosa

**Abstract**—A theoretical model to numerically study the local space-charge field induced by light in a photorefractive crystal biased with two independent, perpendicularly oriented external static fields is introduced. This model appears attractive because it allows varying, in the crystal transverse plane, of the orientation of the external biasing static field with respect to that of the optical-field vector, then enhancing the tensorial properties of the crystal. The numerical analysis has revealed that, in a nonconventional biasing configuration, the spatial distributions of the space-charge-field vector transversal components exhibit a further anisotropy that has not been shown up to now. Nevertheless, from a practical point of view, such a boundary configuration could allow better management of the focusing characteristics of the material.

**Index Terms**—Nonlinear optics, nonlinear wave propagation, optical self-focusing, optical solitons, photorefractive effects, photorefractive materials.

## I. INTRODUCTION

**P**HOTOREFRACTIVE crystals are becoming key materials even in the field of the optical fiber transmission systems. For example, recent literature [1]–[4] carried on a centrosymmetric photorefractive crystal—the potassium lithium tantalate niobate (KLTN)—has shown attractive features of this material, which appears very promising for the realization of advanced optical switches and optical add-drop devices [5], [6]. Moreover, due to the possibility to create, by means of a proper external biasing voltage, a spatial solitonlike waveguide on a photorefractive [7]–[16], intriguing structures for the optical beam manipulation can be obtained as well.

Generally speaking, in a photorefractive medium, a highly diffracting optical beam ionizes impurities hosted in the crystal lattice. An externally applied electric field makes these mobile charges drift to less-illuminated regions, forming a double layer that reduces the resultant electric field in the illuminated region. For an appropriate electrooptic sample, this reduction locally modifies the refractive index and leads to self-lensing so that even soliton propagation is possible to obtain, when the beam diffraction is exactly compensated. It is well known that the characteristics of the waveguide created in a photorefractive

depend on the crystal tensorial structure [8] and on the particular electrooptic response of the crystal to the photo-induced space-charge field that can be linear or quadratic [17], [18]. For noncentrosymmetric structures, the electrooptic refraction-index modulation is proportional to the static space-charge field (linear electrooptic effect, or Pockels effect). In centrosymmetric crystals, the electrooptic response is purely quadratic, and the refractive-index pattern locally induced by light depends on the products of the static space-charge-field vector components (Kerr electrooptic effect).

In this context, the propagation of optical beams in photorefractive crystals belonging to both noncentrosymmetric and centrosymmetric point groups have been extensively studied [7]–[16]. Nevertheless, to the authors' knowledge, most of theoretical and experimental analysis has been performed only according to conventional external biasing schemes, i.e., by considering a transverse external biasing static field just oriented along a given direction, where the electrooptic tensor of the crystal generally exhibits a dominant component. Even when the propagation of optical beams with arbitrary polarization states has been studied [8], different boundary conditions have not been considered. On the contrary, more and more attractive guidance properties of photorefractives could be highlighted if nonconventional boundary configurations are taken in account. In fact, a proper boundary condition, which allows management of the orientation of the external biasing static field with respect to that of the optical-field vector, could enhance the tensorial features of the crystal and allow analysis of its optical confinement properties in a proper way.

This paper describes a numerical analysis of the space-charge-field distribution induced by a visible Gaussian beam in a photorefractive biased with such a nonconventional scheme. Also studied are the characteristics of the local space-charge field in the presence of a rotation of the external biasing static field in the transverse optical beam polarization plane, highlighting the main results that could be useful to evaluate the impact of the boundary on the optical beam propagation. It was found that, by imposing a nonconventional boundary to the crystal, the local space-charge-field distribution—and then the index pattern generated by the active light—can be strongly modified, in such a way as to allow an effective possibility to manage its optical guiding properties. Thus, it is believed that the results reported in this paper could provide useful indications for future theoretical and experimental investigations.

Manuscript received April 15, 2004.

The authors are with CNX S.P.A. Siemens, Località Boschetto, 67100 L'Aquila, Italy.

Digital Object Identifier 10.1109/JLT.2005.849935

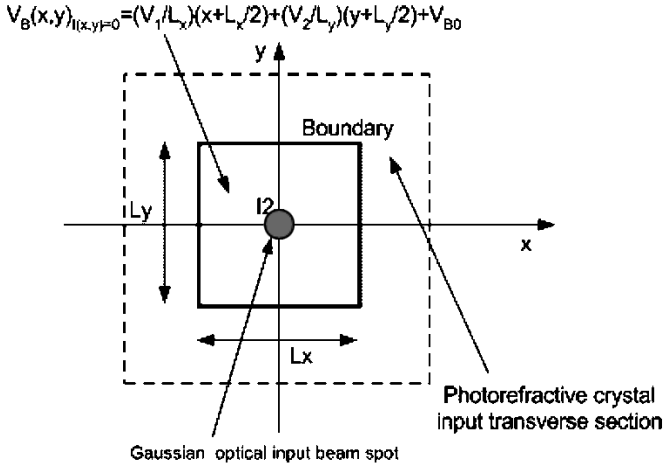


Fig. 1. Theoretical model and boundary conditions.

## II. MATHEMATICAL MODEL

We have performed our analysis of the space-charge field induced by visible light in a biased photorefractive crystal by numerically solving the following Kukhtarev's equation [10], [11]

$$\nabla \cdot \left[ (I + I_B) \nabla \vartheta - \frac{K_B T}{q} \nabla (I + I_B) \right] = 0. \quad (1)$$

In this expression,  $\vartheta(x, y)$  is the electrostatic potential in the  $x$ - $y$  transverse plane,  $I(x, y)$  is the optical intensity of the propagating beam in nonlinear regime,  $I_B$  is the artificial dark irradiance,  $K_B$  is the Boltzmann constant,  $T = 293^\circ$  is the absolute temperature,  $q$  the electron charge, and  $\nabla = ((\partial)/(\partial x), (\partial)/(\partial y))$  is the transverse gradient. For our investigation, we assumed to launch, at the input of the crystal, an optical beam, polarized in the  $x$ - $y$  plane, with a transverse Gaussian spatial intensity distribution given by

$$I(x, y) = I_P \exp \left\{ -\frac{x^2}{2\sigma_x^2} - \frac{y^2}{2\sigma_y^2} \right\} \quad (2)$$

in which  $\sigma_x, \sigma_y$  are the variances along the  $x$  and  $y$  directions, and  $I_P$  the beam peak intensity. In our investigation, we consider a purely transverse (i.e., independent on the  $z$  axis) external biasing-field distribution. In order to analyze the space-charge-field properties in both its  $x$  and  $y$  transverse vector components, we introduced a particular theoretical model (shown in Fig. 1) that allows varying of the orientation of the external biasing static field in the  $x$ - $y$  transverse plane. In this model, we assigned, in correspondence of the transverse section perpendicular to the  $z$  axis, the following boundary conditions for the potential  $\vartheta(x, y)$ :

$$V_B \left( x, y = \pm \frac{L_Y}{2} \right) = \left( \frac{V_1}{L_X} \right) \left( x + \frac{L_X}{2} \right) + V_{B0}, \quad -\frac{L_X}{2} \leq x \leq \frac{L_X}{2} \quad (3a)$$

$$V_B \left( x = \pm \frac{L_X}{2}, y \right) = \left( \frac{V_2}{L_Y} \right) \left( y + \frac{L_Y}{2} \right) + V_{B0}, \quad -\frac{L_X}{2} \leq y \leq \frac{L_X}{2}. \quad (3b)$$

In (3a) and (3b),  $L_X$  and  $L_Y$  are the transversal sizes of the boundary, and  $V_{B0}, V_1, V_2$  the boundary voltage values that are assumed independent on the  $x$  and  $y$  coordinates. From a practical point of view, this approach is equivalent to considering a crystal with transverse sizes much more larger than  $L_X$  and  $L_Y$  that is biased by means of two independent, perpendicularly oriented external static fields, respectively given by  $\vec{E}_X^B(x, y) = -\hat{x}(V_1)/(L_X)$ ,  $\vec{E}_Y^B(x, y) = -\hat{y}(V_2)/(L_Y)$ , when the beam illumination is absent. Moreover, we also assume in this model that the transversal sizes of the boundary are much larger than the beam-spot diameter so that the presence of the optical beam field does not change the distribution of the electric static field at the boundary. According to this approach, we considered an optical beam spot with  $\text{FWHM}_x = \text{FWHM}_y = 10 \mu\text{m}$  (full-width at half-maximum of the optical-field intensity along the  $x$  and  $y$  directions), and transverse boundary sizes  $L_x, L_y$  not less than  $200 \mu\text{m}$ . Now let us make some consideration regarding the structure of (1). We solved the potential equation in (1) by means a five-point finite-difference scheme. In this theoretical model, the space-charge-field distribution is given by the contribution of the drift and the diffusive fields [10], [11], [19], [20]. Generally speaking, for a given boundary condition (3a) and (3b), the solution of (1) can be expressed as the superposition of two terms: the solution of the homogeneous equation

$$\nabla \cdot [(I + I_B) \nabla \vartheta] = 0 \quad (4)$$

with the boundary conditions (3a) and (3b), and the solution of the inhomogeneous equation (1), in which the boundary condition

$$V_B \left( x, y = \pm \frac{L_Y}{2} \right) = 0, \quad -\frac{L_X}{2} \leq x \leq \frac{L_X}{2} \quad (5a)$$

$$V_B \left( x = \pm \frac{L_X}{2}, y \right) = 0, \quad -\frac{L_X}{2} \leq y \leq \frac{L_X}{2} \quad (5b)$$

is imposed. We can derive the drift-field vector components from the homogeneous equation (4), with the conditions (3a) and (3b), and the diffusion-field vector components from the inhomogeneous equation (1) by means of (5a) and (5b). Then, for each transverse vector component, the complete space-charge-field distribution induced by the Gaussian beam is given by the superposition of two vector-field distributions: an anisotropic-field spatial distribution like that reported in literature [15], which gives the space-charge field induced by the drift of the space charges and a purely asymmetric-field spatial distribution due to the presence of the diffusive term. An immediate consequence of this feature of (1) is that different orientations and magnitudes of the external biasing static field induce changes only on the anisotropic space-charge field distribution, without any impact on the diffusive term. Moreover, we can express the space-charge-field vector components as

$$\vec{E}_X(x, y) = \hat{x}E_X(x, y) = \hat{x}E_X^{\text{DRIFT}}(x, y) + \hat{x}E_X^{\text{DIFF}}(x, y) \quad (5a)$$

$$\vec{E}_y(x, y) = \hat{y}E_y(x, y) = \hat{y}E_y^{\text{DRIFT}}(x, y) + \hat{y}E_y^{\text{DIFF}}(x, y) \quad (5b)$$

where the notations DRIFT and DIFF refer to the drift and the diffusion fields, respectively. As we will show in the following analysis, this consideration allows us to better evaluate the impact of both drift and diffusive terms on the features of the photorefractive crystal. In this sense, one should specify the form of the crystal electrooptic tensor, which can be linear or quadratic [17]. According to the structure of the crystal electrooptic tensor, in a biased photorefractive medium, the space-charge-field distribution induced by the visible beam modifies the refractive-index pattern, thereby changing the propagation features of the beam that propagates through the crystal [7]–[15]. The general tensorial problem is rather complicated and leads to coupled equations for the polarization components of the optical field [8]. This problem is beyond the scope of this paper, and we limit ourselves to qualitatively describing the impact of the space-charge field induced by the photorefractive effect on the beam propagation through the crystal. In a complete tensorial approach, the ratio between refractive-index modulation depth and the zero-field refractive indexes is very small so that a series expansion can be performed [10], [11], [17], and all nonlinear terms in the coupled nonlinear equation [8] are commonly considered linearly proportional (noncentrosymmetric crystals [10], [11]) or quadratically proportional (centrosymmetric crystals [17]) to the magnitude of the vector components of the space-charge field. Because we mainly aim to analyze the vector properties of the static photorefractive space-charge field in standard and nonstandard biasing conditions, without a significant lack of generality, we generically describe the impact of the space-charge-field vector components on the beam propagation by means of the simplified expressions

$$\Delta n(x, y) = n(x, y) - n_0 = -a \cdot E_i(x, y) \quad (6a)$$

$$\Delta n(x, y) = n(x, y) - n_0 = -b \cdot E_i(x, y)E_j(x, y). \quad (6b)$$

In (6a) and (6b), valid for noncentrosymmetric and centrosymmetric crystals, respectively,  $n_0$  is the zero-field refractive index (which generally is one of the principal indexes), and both indexes  $i, j$  can be set equal to the  $x$  and  $y$  transverse coordinates.  $\Delta n(x, y)$  is the generic nonlinear term associated to the refractive-index modulation, and  $n(x, y)$  is the local refractive-index spatial distribution induced by the vector space-charge-field components that are taken in account. The constants  $a$  and  $b$  are assumed positive and, in practice, can be considered proportional to the coefficients of the linear and quadratic electrooptic tensors that are taken in account, according to the beam-launching conditions and the geometry of the medium. Then, by means of the (6a) and (6b), we analyze separately the features of each nonlinear term that can be present in the coupled nonlinear equations describing the beam propagation through photorefractives.

### III. SPACE-CHARGE FIELD INDUCED BY A GAUSSIAN BEAM IN A CONVENTIONAL BIASING SCHEME

We considered the square input transverse section of the photorefractive crystal, biased along the  $x$  transverse direction with an external static field  $|\vec{E}^B(x, y)| = |\vec{E}_X^B(x, y)| = 2.3 \cdot 10^5$  V/m, in which a visible optical input Gaussian beam induces a local space-charge-field distribution. We analyzed the characteristics of the photogenerated space-charge field by varying both the orientation of the external biasing static-field vector and the normalized input beam peak intensities ratio  $I/I_B$ . We first studied the local-field distribution obtained by imposing  $I/I_B = 2.6$ .

Fig. 2(a) shows the numerical evaluation of the  $E_x(x, y)$  component of static electric field associated to the input Gaussian beam with the parameters reported previously (in all figures reported here, a.u. stands for *arbitrary units*). The space-charge field induced by the Gaussian beam appears highly anisotropic. It exhibits a major central lobe and two lateral smaller lobes oriented along the  $x$  axis. The peak amplitudes of the lobes are equal to  $\approx 1.2 \cdot 10^5$  V/m (central lobe) and  $\approx 4 \cdot 10^4$  V/m (lateral lobes), versus a plateau value of  $\approx 2.3 \cdot 10^5$  V/m (this last term corresponds to the value of the electric static field when the input optical beam is absent).

We report in Fig. 2(b) the  $x$  component of the diffusive field. It exhibits an evident asymmetry along the  $x$  direction. Therefore, due to the presence of the diffusion field that overlaps to the drift field, the whole space-charge-field distribution undergoes a small lack of symmetry along the  $x$  direction, and then the amplitudes of lateral lobes are slightly different.

Now let us consider a conventionally biased noncentrosymmetric crystal [8], [10], [11]. According to the simplified expression (6a), the drift term of the space-charge field  $x$  component in Fig. 2(a) modifies the refractive-index pattern that, in proximity of the beam spot, exhibits a main central lobe and two smaller lateral lobes. This leads to an increase of the refractive index in the beam center region, where a *graded-index waveguide* is created, and the beam is focused through the propagation.

With regard to the diffusive field  $E_X^{\text{DIFF}}(x, y)$ , literature based on the study of the optical beam propagation in photorefractives has shown that it induces a self bending of an optical beam that propagates through the crystal [19]–[22]. This feature of the diffusive-field component can be explained by means of the small lack of symmetry along the  $x$  direction introduced by this term in the space-charge-field distribution. For example, recalling (6a), in the case of a conventionally biased noncentrosymmetric crystal, according to the spatial distribution reported in Fig. 2(a), the ends of the center region of the graded-index waveguide due to the photorefractive effect must exhibit two lateral holes along the  $x$  axis, having different depths along the  $x$  direction. Thus, the waveguide due to the space-charge field induces two slightly different focusing effects on the lateral ends of the beam along the  $x$  axis, giving rise to a beam bending during the propagation. The beam bending is just oriented along the direction of these lateral wells and directed toward those that are less deep, where the focusing effect on the beam lateral endings along the  $x$  direction is lower.

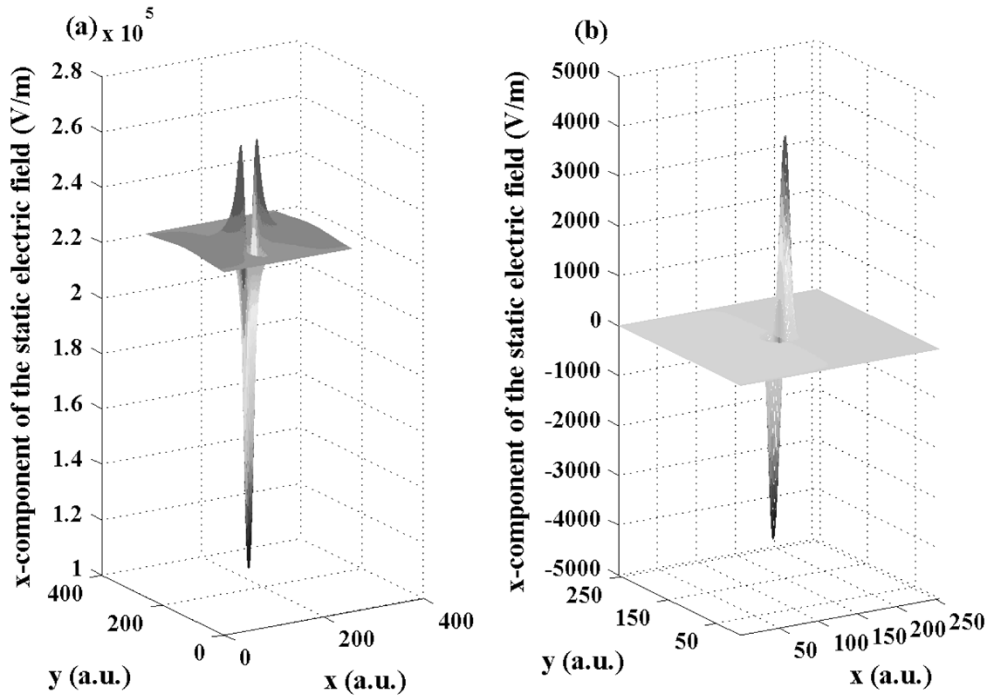


Fig. 2. Conventional biasing scheme with  $|\vec{E}^B(x, y)| = |\vec{E}_X^B(x, y)| = 2.3 \cdot 10^5$  V/m. (a)  $x$  component of the space-charge field  $E_X(x, y)$ . (b)  $x$  component of the diffusive field  $E_X^{DIFF}(x, y)$ .

Now we consider the structure of the  $y$  component  $E_Y(x, y)$  [shown in Fig. 3(a)]. It exhibits a different shape with respect to the  $x$  component, characterized by a quite complicated anisotropic four-lobe structure, with two couples of positive and negative lobes versus a plateau value of 0 V/m. From numerical calculation, it emerges that the amplitudes of these four lobes ( $\approx \pm 4.5 \cdot 10^4$  V/m) are around 20% of the plateau value of the  $E_x(x, y)$  component and of the same order of magnitude of its two lateral smaller sidelobes [shown in Fig. 2(a)].

As in the case of the other transverse component, the structure of the  $y$  component of the static electric field induced by the light depends on the  $y$  component of the diffusive field, shown in Fig. 3(b). We note that this component is asymmetric along the  $y$  direction. Then, it induces on the anisotropic four-lobe structure a further slight asymmetry along the  $y$  axis so that, within each couple of lobes having the same sign, the amplitudes appear slightly different.

As reported previously, the impact of  $E_Y(x, y)$  on the beam evolution in the photorefractive crystal consists on two contributions: the drift  $E_y^{DRIFT}(x, y)$  and the diffusive  $E_y^{DIFF}(x, y)$  components. From a rigorous point of view, we can expect that, according to the structure of the electrooptic tensor (linear or quadratic), the drift field *perturbs* the beam propagation through the crystal by modifying the guidance properties of the waveguide that itself induces. With regard to the diffusive field  $E_Y^{DIFF}(x, y)$ , it introduces a further slight lack of symmetry in the  $E_Y(x, y)$  component, and then the contribution of  $E_Y(x, y)$  could give rise to a further beam bending of the optical beam during the propagation. Clearly, the particular impact of this vector component depends on the structure of the electrooptic tensor of the crystal but, with the help of (6a), we can make

some useful consideration about the symmetry characteristics of this vector space-charge-field component.

Therefore, let us consider Fig. 3(b). According to (5b), the  $y$  component of the space-charge field is due to the superposition of both drift and diffusive terms. Because the diffusive-field  $y$  component exhibits an asymmetry along the  $y$  axis, we have that, in this figure, the peak amplitude of the positive lobe closer to the (0, 0) origin is lower than the other, far from the origin, and the peak of the negative lobe closer to the  $y$  axis is less negative in comparison with its twin.

For a noncentrosymmetric sample, we apply (6a) and analyze the features of a graded-index waveguide induced by a refractive-index modulation linearly proportional to the  $E_y(x, y)$  term (still assuming a positive proportionality constant). In this case, from a theoretical point of view, among all lobes in the space-charge-field  $y$  component distribution, only the positive lobes produce a confinement effect on the optical beam. In fact, in the direction along the positive lobes, the optical beam *sees* a locally modified refractive-index distribution, in which two lateral small holes are introduced. Then, along the positive lobes, the beam *sees* lateral refractive-index values that are lower than those in proximity of the beam peak intensity and induce a focusing effect on it. The situation is practically inverted in the direction along the negative lobes that introduce an antiguiding effect on the beam. Because in this configuration only the positive lobes produce a confinement of the beam, what effectively induces the beam bending through the propagation is the asymmetry of the positive lobes. In fact, due to the asymmetry induced by the diffusive term, in the direction along the negative lobes the depths of the lateral holes in the refractive-index pattern are slightly different, and this

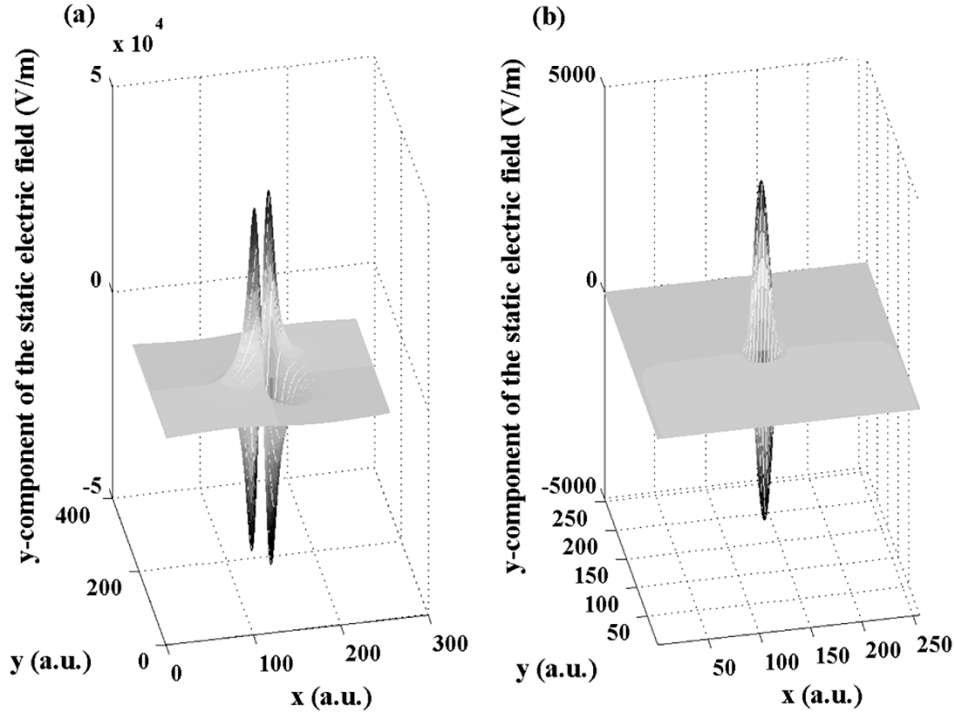


Fig. 3. Conventional biasing scheme with  $|\vec{E}^B(x, y)| = |\vec{E}_X^B(x, y)| = 2.3 \cdot 10^5$  V/m. (a)  $y$  component of the space-charge field  $E_Y(x, y)$ . (b)  $y$  component of the diffusive field  $E_Y^{\text{DIFF}}(x, y)$ .

feature produces a bending of the propagating beam. On the contrary, the asymmetry of the negative antiguiding lobes do not affect the propagation through the crystal, and then only the  $y$  component of the space-charge field effectively produces an effective beam bending, just along the direction oriented along the positive lobes. Generally speaking, according to the beam-launching conditions and to the characteristics of the electrooptic tensor of the medium, both  $x$  and  $y$  components of the diffusive term can interact with each other, and the resulting beam bending is given by a mixture of their separated contributions.

In the case of centrosymmetries [17], the beam evolution is given by the quadratic terms  $E_X^2(x, y)$ ,  $E_Y^2(x, y)$  and by the product  $E_X(x, y)E_Y(x, y)$ . The spatial distribution of  $E_X^2(x, y)$  exhibits the same shape and asymmetry of the case in Fig. 2(a) so that, in the frame of the scalar simplified approach of (6b), with a positive proportionality constant, it produces a confinement effect on the beam and induces a beam bending in the same direction. The cases of the quadratic term  $E_Y^2(x, y)$  and the product  $E_X(x, y)E_Y(x, y)$  are quite anomalous. In this sense, we noticed from simulations that the  $E_Y^2(x, y)$  term shows a four-lobe structure in which all lobes are positive, as we could reasonably expect by its quadratic expression. Nevertheless, this term did not show an asymmetry along the  $y$  direction, as we could expect from the presence of the diffusive field, but the same asymmetry of  $E_X^2(x, y)$ , i.e., oriented along the  $x$  axis. This is because, according to (5b), the asymmetry is introduced in the quadratic expression of  $E_Y^2(x, y)$  through the product  $2E_Y^{\text{DRIFT}}(x, y)E_Y^{\text{DIFF}}(x, y)$ , which combines the features of both drift and diffusive terms. By considering, according to (6b), a graded-index waveguide induced by a refractive-index modulation proportional to the  $E_Y^2(x, y)$  term, all four lobes in the

$y$  component structure produce a confinement effect on the optical beam, and the effective asymmetry in the  $E_Y^2(x, y)$  term should enhance the beam bending in the direction of the external biasing field. Finally, with regard to the characteristics of the  $E_X(x, y)E_Y(x, y)$  spatial distribution, numerical simulations showed that it appears analogous to that of the  $E_Y(x, y)$  term in Fig. 3(a), so that we can extend to it the same considerations expressed previously for this vector component.

Now we consider the local space-charge-field distribution in the saturation regime, i.e., with very low values of the background optical intensity. We imposed a normalized beam intensity ratio equal to  $I/I_B = 2.6 \cdot 10^{-6}$  and the same value of the external biasing field. We show the results in Figs. 4 and 5, reporting the  $E_X(x, y)$  and  $E_Y(x, y)$  spatial distributions, respectively. In order to analyze these features, we must take in account that the contribution of the diffusive term to the space-charge field strongly depends on the derivatives of the optical beam intensity distribution and becomes more and more significant by increasing the normalized beam intensity ratio and decreasing the optical beam spot radius. Then, in a strong saturation regime, it can become a dominant term in both  $E_X(x, y)$  and the  $E_Y(x, y)$  components. Owing to this consideration, we solved the homogeneous equation (4), with the boundary conditions (3a) and (3b), thus by neglecting the presence of the diffusive field.

Fig. 6(a) and (b) shows the  $x$  and  $y$  components of the drift field in the conventional biasing situation. In comparison with the case of Fig. 2, we can note an evident saturation effect on the major central lobe of the space-charge-field  $x$  component [Fig. 6(a)]. This behavior of the drift field in the saturation regime exhaustively explains the lack of guidance in a biased photorefractive crystal in presence of low optical

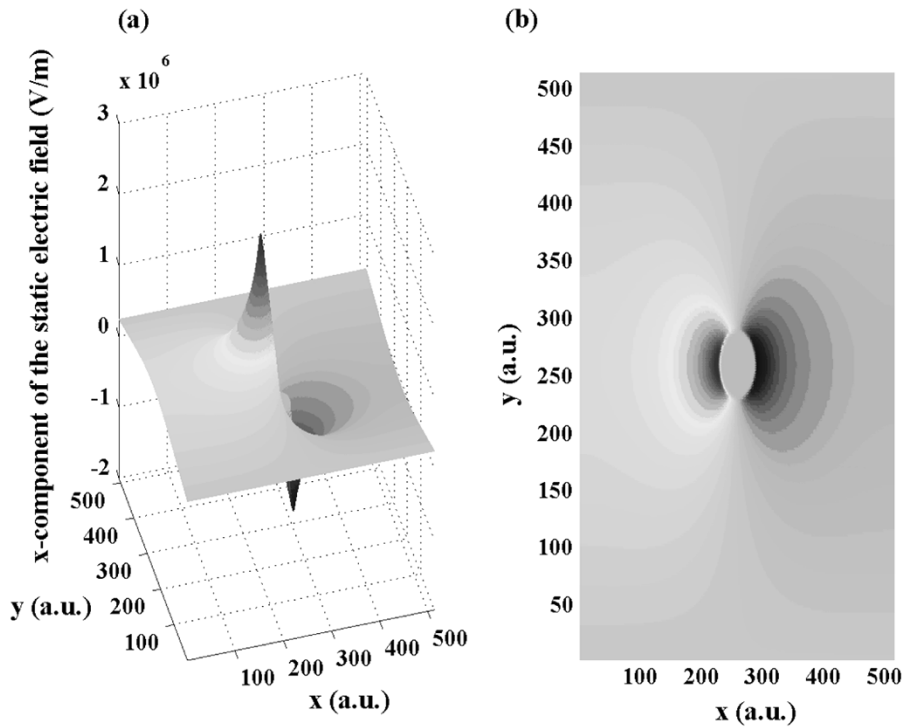


Fig. 4. Conventional biasing scheme with  $|\vec{E}^B(x, y)| = |\vec{E}_X^B(x, y)| = 2.3 \cdot 10^5$  V/m.  $x$  component of the saturated space-charge field  $E_X(x, y)$ : (a) side view and (b) top view.

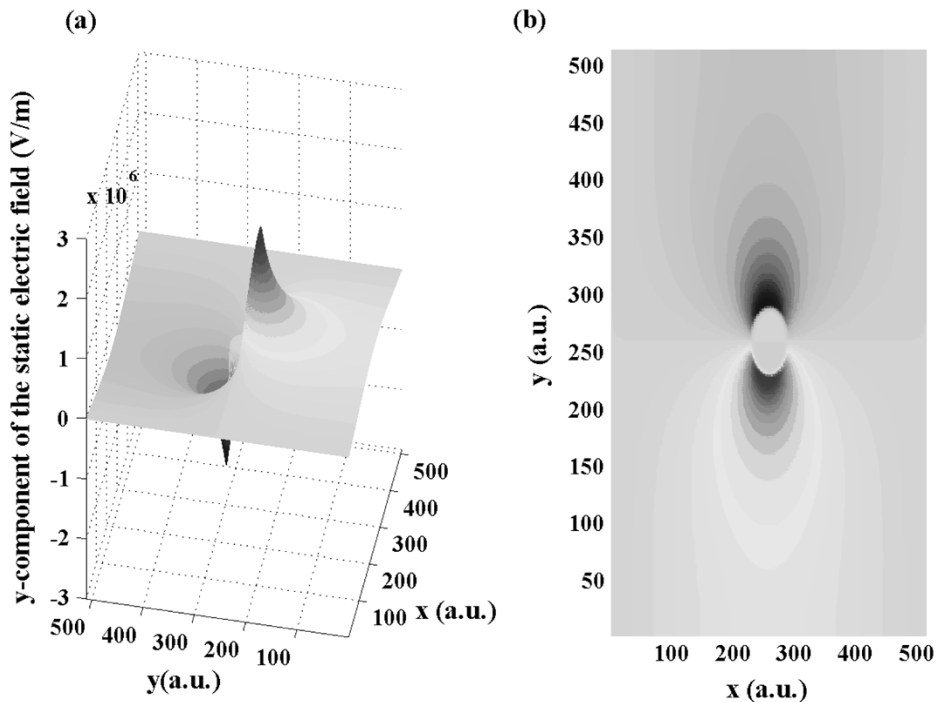


Fig. 5. Conventional biasing scheme with  $|\vec{E}^B(x, y)| = |\vec{E}_Y^B(x, y)| = 2.3 \cdot 10^5$  V/m.  $y$  component of the saturated space-charge field  $E_Y(x, y)$ : (a) side view and (b) top view.

backgrounds. In fact, from Fig. 6(a), it emerges that, by increasing the normalized beam intensity ratio, the main central lobe exhibits a pseudoelliptical *flattened* shape that induces a local refractive-index pattern practically constant over a large region of the  $x$ - $y$  plane. This portion of space is quite larger than the Gaussian beam spot so that the guiding effect of the refractive-index modulation disappears. Obviously, this

consideration does not take in account the contribution of the diffusive field. A comparison with Figs. 4 and 5 shows that, at very low values of the background intensity plateau, the diffusive-field components can be even an order of magnitude larger than the corresponding drift amplitudes, thus confirming the importance of the diffusive term on the total space-charge field in this operating regime.

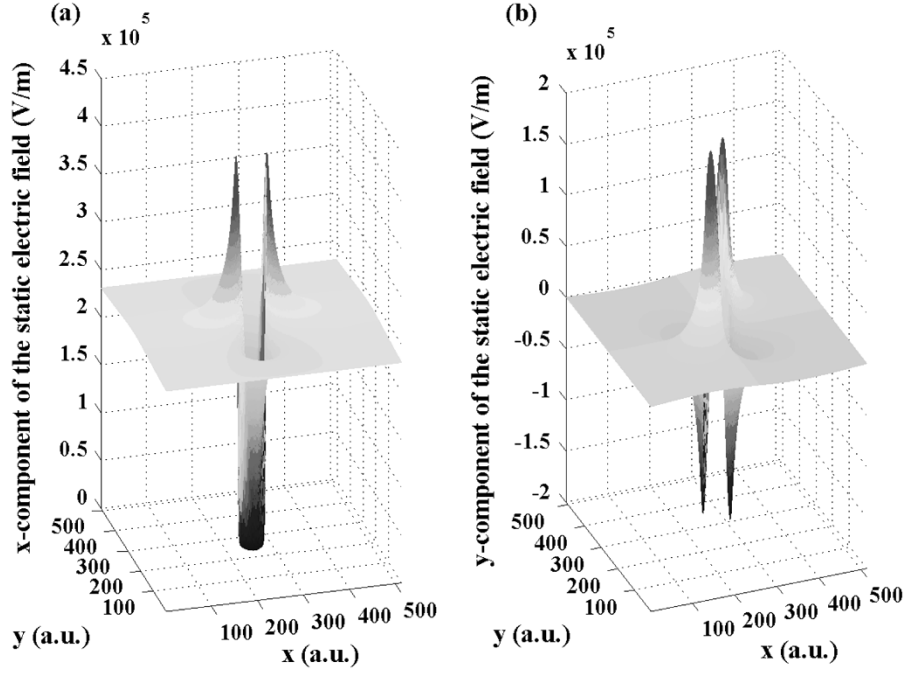


Fig. 6. Conventional biasing scheme with  $|\vec{E}^B(x, y)| = |\vec{E}_X^B(x, y)| = 2.3 \cdot 10^5$  V/m. Saturated space-charge drift field: (a)  $xx$  component  $E_X^{\text{DRIFT}}(x, y)$  and (b)  $y$  component  $E_Y^{\text{DRIFT}}(x, y)$ .

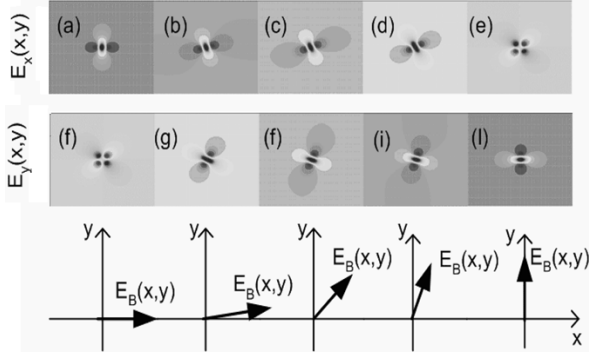


Fig. 7. Nonconventional biasing schemes by varying the orientation of the biasing field  $\vec{E}^B(x, y)$  in the upper right quadrant. (a)–(e)  $x$  component of the space-charge field  $E_X(x, y)$ . (f)–(l)  $y$  component of the space-charge field  $E_Y(x, y)$ .

#### IV. SPACE-CHARGE FIELD INDUCED BY A GAUSSIAN BEAM IN A NONCONVENTIONAL BIASED SCHEME

Now we will analyze the space-charge-field distribution induced by a particular boundary condition, where the external biasing field vector rotates in the  $x$ – $y$  transverse plane. It is an intriguing investigation because, with this new configuration, from a theoretical point of view, we could expect to enhance the focusing properties of the  $E_Y^{\text{DRIFT}}(x, y)$  or modify the impact of the lack of symmetry induced on the space-charge field by the diffusive-term vector components. Figs. 7(a)–(l) and 8(a)–(l) show the transverse space-charge-field distributions corresponding to a complete rotation of the external static biasing static-field vector in the  $x$ – $y$  plane. Fig. 7(a) and (f) report the same biasing condition of Fig. 2(a) and (b), where the biasing field is applied only on the  $x$  direction. In the  $x$ – $y$  transverse plane, the  $x$  component of the space-charge field exhibits a

pseudoelliptical shape of the major central lobe, squeezed along the  $x$  axis [23]. From the subsequent figures, it emerges that, with the same magnitude of the external biasing field, by increasing the contribution of the  $y$  component  $\vec{E}_Y^B(x, y)$ , both distributions of the  $x$  and  $y$  components of the space-charge field gradually change in a significant way. Progressively, the  $x$  component  $E_x(x, y)$  is driving to get the same asymmetric four-lobe structure of the  $E_y(x, y)$  component in the case of an  $x$ -biased crystal [Fig. 3(a)]. We can note this feature simply by comparing Fig. 7(e) with Fig. 7(f): the distribution of maxima and minima is the same for both cases. Nevertheless, the asymmetry induced by the diffusive term introduces a difference between the two space-charge-field components. In fact, in the case of Fig. 7(e), the diffusive  $x$  component  $E_X^{\text{DIFF}}(x, y)$  overlaps to the  $x$  component  $E_X^{\text{DRIFT}}(x, y)$  and induces an asymmetry along the  $x$  axis. On the contrary, in the case of Fig. 7(f), the diffusive  $y$  component  $E_Y^{\text{DIFF}}(x, y)$  overlaps to the  $y$  component  $E_Y^{\text{DRIFT}}(x, y)$ , and then an asymmetry along the  $y$  axis appears. On the other hand, by making a comparison between Figs. 7(a) and (l), we can note that the  $y$  component of the space-charge field gradually assumes a feature analogous to that of the  $x$  component in Fig. 2(a). Nevertheless, we note that the orientation of the two lateral smaller lobes appear different, as well as the *squeezings* of both major central lobes, each one oriented along the external biasing-field direction. With regard to the intermediate cases, Fig. 7(b)–(d) and (g)–(i) show that, by gradually changing the external biasing-field vector orientation, the space-charge-field components exhibit a mixing of behaviors reported here previously. For example, by looking at Fig. 7(b) and (g), where the external biasing-field vector is rotated  $\approx 0.40$  rad with respect to the  $x$  axis, we note that the contribution of the biasing-field  $y$  component produces a slight rotation of the  $x$  component of the space-charge field, and a merging

of the guiding lobes in the space-charge-field  $y$  component that overlap each other and form a pseudoelliptical guiding central lobe. The situation results are practically inverted in Fig. 7(d) and (i), where the external biasing-field vector is rotated up to  $\approx 1.16$  rad with respect to the  $x$  axis.

Fig. 7(c) and (h) are probably the most significant, from a practical point of view. In fact, in this case, the biasing static electric-field vector is oriented at  $\pi/4$  rad with respect to the  $x$  axis, and then the crystal undergoes a particular boundary condition, with  $|E_X^B(x, y)| = |E_Y^B(x, y)| = (1/\sqrt{2}) \cdot 2.3 \cdot 10^5$  V/m. The presence of such a boundary scheme removes the anisotropy shown in Fig. 7(e) and (f), concerning the drift component of both space-charge-field vector components in the case of a conventional biasing scheme. In fact, both distributions basically exhibit the same structure, analogous to that reported in Fig. 2(a) for the conventional biasing scheme, with a plateau field, a pseudoellipsoidal major central lobe, and two lateral smaller lobes. In comparison with the structure in Fig. 2(a), we have that the plateau level and the peak amplitudes of the lobes in each distribution are reduced by a  $\sqrt{2}$  factor (as we reasonably expect). Nevertheless, in this biasing conditions, the space-charge field shows a different aspect of its anisotropic nature. A further particular anisotropy of the space-charge field appears from Fig. 7(c) and (h): the spatial distributions of  $E_X(x, y)$ ,  $E_Y(x, y)$  clearly show two different orientations of the central lobe *squeezed* axes. This lack of isotropy concerns the drift components  $E_X^{\text{DRIFT}}(x, y)$ ,  $E_Y^{\text{DRIFT}}(x, y)$  of the total space-charge field.

As in the case of the previous section, the whole spatial structure of each vector component can be described as the superposition of the drift and the diffusion terms. The asymmetric diffusion-field vector components overlap on the drift vector terms introducing, in each vector component spatial distribution, an effective asymmetry oriented along the *squeezed* axes of the central pseudoellipsoidal distributions, making the lateral lobes slightly different. Then, let us consider a noncentrosymmetric crystal in such a nonconventional biasing condition. As in the last section, for sake of simplicity, let us introduce the simplified scalar approach of the (6a) and analyze the properties of the graded-index waveguides induced by the refractive-index modulation linearly proportional to the  $E_x(x, y)$  and  $E_y(x, y)$  term, respectively. By still assuming a positive proportionality constant, from the considerations expressed previously, we derive that each local-field vector component (separately considered) behaves as in the case of Fig. 2(a), thus leading to an increase of the refractive index in the beam center region so that a beam confinement is achieved. Moreover, the asymmetry due to the diffusive term also acts as in the case of Fig. 2(a) and then induces a beam bending just along a direction parallel to the *squeezed* axis of its own central lobe.

In the case of centrosymmetric structures, with this boundary configuration, the squared terms  $E_X^2(x, y)$ ,  $E_Y^2(x, y)$  exhibit the same shapes and asymmetries of the  $E_x(x, y)$ ,  $E_y(x, y)$  distributions, and then, for these terms with the same sign of the proportionality constant, the same considerations reported previously for a noncentrosymmetric sample can be made. With regard to the product  $E_X(x, y)E_Y(x, y)$ , the numerical simulation showed that also the spatial distribution of the

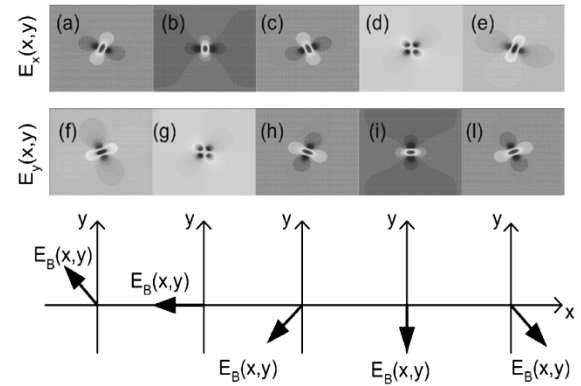


Fig. 8. Nonconventional biasing schemes by varying the orientation of the biasing field  $\vec{E}^B(x, y)$  in the upper left, lower left, and lower right quadrants. (a)–(e)  $x$  component of the space-charge field  $E_X(x, y)$ . (f)–(l)  $y$  component of the space-charge field  $E_Y(x, y)$ .

product  $E_X(x, y)E_Y(x, y)$  appears similar to those of the terms  $E_X(x, y)$ ,  $E_Y(x, y)$ , with a main pseudoellipsoidal central lobe and two lateral smaller lobes. However, in this case, the orientation of the central lobe *squeezed* axis is between the directions of the  $E_X(x, y)$ ,  $E_Y(x, y)$  central lobes *squeezed* axes, with the same asymmetry characteristics. Then, with the same previously mentioned assumptions, this term should also induce a confinement of the beam through the propagation, as well as a self-bending mainly oriented along a direction parallel to the *squeezed* axis of its own central lobe.

These features appear interesting because it confirms that, from a theoretical point of view, by means of a proper nonconventional biasing configuration, the impact of both external biasing static-field vector components can be enhanced, and then both space-charge-field vector components can be used to manage the focusing properties of the photorefractive medium, especially in the case of arbitrarily polarized input optical beams. In particular, such a nonconventional biasing scheme could be particularly attractive to manage vector photorefractive spatial solitons. In this context, according to the results in [8], self-coupled (i.e., coupled only through the dependence of the space-charge field on the optical intensity) and cross-coupled (i.e., coupled through the electrooptic tensor and the space-charge field) vector solitons, or a combination of them as well, may exist. In a conventional biasing scheme, the two polarizations of the vector solitons may be coupled, according to correct phase matching and specific configurations. A nonconventional biasing configuration could enhance the coupling capabilities in both vector soliton classes, offering new opportunities for the use of the photorefractive materials. Nevertheless, such a particular boundary condition also shows a further anisotropy of the space-charge field that has not been revealed up to now. Generally speaking, we expect that, according to a given (linear or quadratic) tensorial structure of the electrooptic tensor of a crystal, the electric-field transverse vector components of an optical Gaussian beam that propagates in a nonconventional biased photorefractive medium *see* different waveguides, each one of them having a different orientation of the central lobe *squeezed* axis. Because this anisotropy is clearly not negligible *a priori*, it must be taken into account in describing the beam propagation along a non-

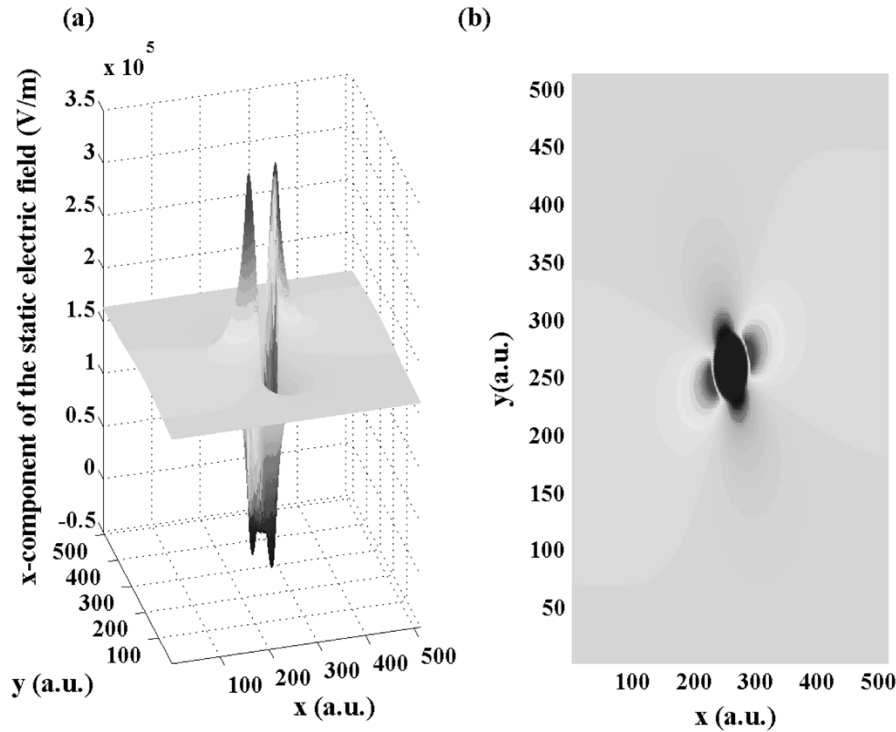


Fig. 9. Nonconventional biasing scheme with  $|E_X^B(x, y)| = |E_Y^B(x, y)| = (1/\sqrt{2}) \cdot 2.3 \cdot 10^5$  V/m.  $x$  component of the saturated space-charge field  $E_X(x, y)$ : (a) side view and (b) top view.

conventional biased crystal. We expect that it is especially true in the case of vector spatial solitons or, according to a more realistic approach, when the adiabatic evolution of the Gaussian beam transverse polarization states in optical vector spatial solitons is analyzed [19], [20]. We do not address this particular problem here, but we think that this result could give rise to further intriguing investigations about this theme.

In Fig. 8(a)–(l), we observe the remaining cases regarding the evolution of the space-charge-field vector components, when the external biasing-field vector is gradually rotated, with a step of  $\pi/4$  rad, in the  $x$ – $y$  transverse plane up to the lower right quadrant, where it performs an angle of  $-(\pi/4)$  rad with the  $x$  axis. We can note that the lobes of the vector components progressively invert their sign, and then change the confinement properties of the waveguides that can be induced in the crystal, and the beam bending direction as well. This is particularly true in a noncentrosymmetric crystal, where the dependence of the nonlinear effect on the space-charge field is linear, but can be significant in a centrosymmetric as well, if the optical input polarization state is arbitrary, and a nonconventional biasing configuration is used. In fact, in this case, the product of the components  $E_X(x, y)E_Y(x, y)$ , as well as the coupling between the optical-field transverse components, is sign dependent.

As in the previous section, now we study the local space-charge-field distribution in the saturation regime ( $I/I_B = 2.6 \cdot 10^{-6}$ ), in the case of a nonconventional scheme. Among all cases reported up now, we analyze the symmetric boundary condition reported in Fig. 7(c) and (h), where the biasing static electric-field vector is oriented at  $\pi/4$  rad with respect to the  $x$  axis. Then, we compare the results obtained with those reported in Figs. 4–6 for a conventionally biased crystal.

As we could expect from the considerations expressed in the previous section, the numerical analysis performed in the nonconventional biasing scheme showed that, in comparison with the previous case, the  $E_X(x, y), E_Y(x, y)$  space-charge-field components distributions do not change in a significant way, when the external biasing-field vector rotates in the  $x$ – $y$  plane, because the diffusion term is still dominant. Then, we have still performed a numerical analysis of the drift field (given by the homogeneous equation (4), by imposing (3a) and (3b)). Figs. 9(a) and (b) and 10(a) and (b) report the corresponding results for the nonconventional biasing configuration. We can note that, in this other scheme, the saturation mechanism affects both central lobes belonging to the drift field  $x$  and  $y$  components, which exhibit more sophisticated spatial structures, in comparison with those reported in Fig. 6(a) and (b). Apart from two small lobes, which should not introduce a significant impact on the beam propagation, both structures still show a central *flattened* spatial distribution of the space-charge field, which induces a local refractive-index pattern practically constant over a portion of space in the  $x$ – $y$  plane larger than the Gaussian beam spot, thus compromising the guiding effect of the refractive-index modulation.

As we have already mentioned, this feature of the drift field is practically negligible, in the case of a strong saturation regime, because the impact of the diffusive field is clearly dominant. Nevertheless, in spite of the large impact of the diffusive field on the total space-charge-field distribution, even in the case of the strong saturation regime, the drift vector components keep their anisotropic nature, with each one of them having a different orientation of the central lobe squeezed axis. This result agrees with the theoretical approach introduced in the previous section,

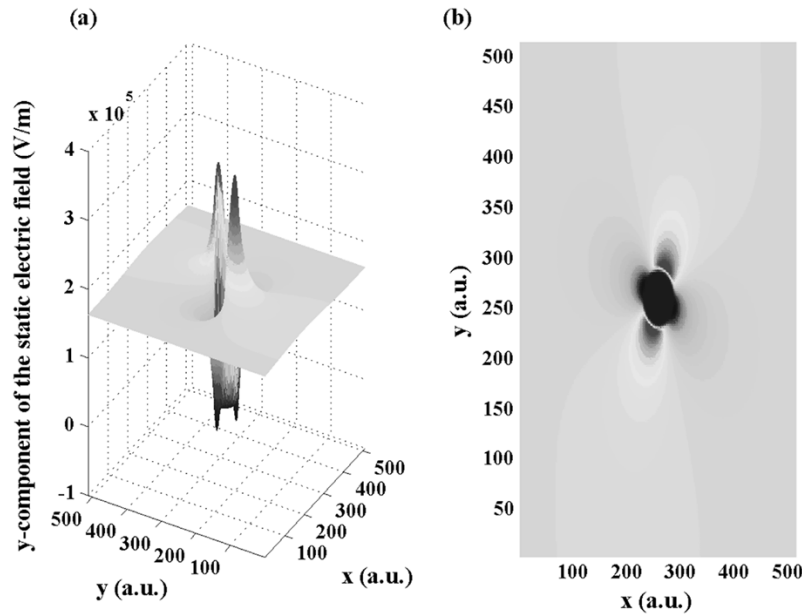


Fig. 10. Nonconventional biasing scheme with  $|E_X^E(x, y)| = |E_Y^E(x, y)| = (1/\sqrt{2}) \cdot 2.3 \cdot 10^5$  V/m.  $y$  component of the saturated space-charge field  $E_Y(x, y)$ : (a) side view and (b) top view.

by means of Figs. 5(a) and (b), which derives all properties of the space-charge field induced by visible light in a photorefractive through a superposition of the drift and diffusive-fields vector components.

## V. CONCLUSION

A nonconventional biasing configuration induces significant changes in the spatial distributions of the space-charge-field vector transversal components, introducing different anisotropic features in its structure. In any case, such a boundary configuration appears attractive to consider, because it could allow to manage the impact of both external biasing static-field vector components on the local space-charge field, and then control the focusing properties of the photorefractive medium in the case of arbitrarily polarized input optical beams.

## ACKNOWLEDGMENT

The authors would like to thank S. Saracino for his precious cooperation and G. De Marzi for his continuous encouragement.

## REFERENCES

- [1] S. Lan, E. DelRe, Z. Chen, M. Shih, and M. Segev, "Directional coupler with soliton-induced waveguides," *Opt. Lett.*, vol. 24, pp. 475–477, 1999.
- [2] E. DelRe, B. Crosignani, P. Di Porto, E. Palange, and A. J. Agranat, "Electro-optic beam manipulation through photorefractive needles," *Opt. Lett.*, vol. 27, pp. 2188–2190, 2002.
- [3] D. Haertle, G. Caimi, A. Haldi, G. Montemezzani, P. Gunter, A. A. Grabar, I. M. Stoika, and Y. M. Vysochanskii, "Electro-optical properties of  $\text{Sn}_2\text{P}_2\text{S}_6$ ," *Opt. Commun.*, vol. 215, no. 4–6, pp. 333–343, 2003.
- [4] G. M. Tosi-Beleffi, F. Curti, D. Boschi, C. Palma, and A. J. Agranat, "Soliton-based Y-branch in photorefractive crystals induced through dispersion-shifted optical fiber," *Opt. Lett.*, vol. 28, pp. 1561–1563, 2003.
- [5] A. J. Agranat, M. Razvag, and M. Balberg, "Dipolar holographic gratings induced by the photorefractive process in potassium lithium tantalate niobate at the paraelectric phase," *J. Opt. Soc. Amer. B, Opt. Phys.*, vol. 14, pp. 2043–2048, 1997.
- [6] A. J. Agranat, E. Littwitz, M. Razvag, and A. Rubissa, "Electroholographic wavelength selective photonic switch for WDM routing," PCT Patent WO 01/07 946 A1, Feb. 1, 2001.
- [7] M. Morin, G. Duree, G. Salamo, and M. Segev, "Waveguide formed by quasi-steady-state photorefractive spatial solitons," *Opt. Lett.*, vol. 20, pp. 2066–2068, 1995.
- [8] M. Segev, G. C. Valley, S. R. Singh, M. I. Carvalho, and D. N. Christodoulides, "Vector photorefractive spatial solitons," *Opt. Lett.*, vol. 20, pp. 1764–1766, 1995.
- [9] M. Shih, Z. Chen, M. Mitchell, M. Segev, H. Lee, R. S. Feigelson, and J. P. Wilde, "Waveguides induced by photorefractive screening solitons," *J. Opt. Soc. Amer. B, Opt. Phys.*, vol. 14, pp. 3091–3100, 1997.
- [10] B. Crosignani, P. Di Porto, A. Degasperis, M. Segev, and S. Trillo, "Three-dimensional optical beam propagation and solitons in photorefractive crystals," *J. Opt. Soc. Amer. B, Opt. Phys.*, vol. 14, pp. 3078–3090, 1997.
- [11] B. Crosignani, P. Di Porto, M. Segev, G. Salamo, and A. Yariv, "Photorefractive spatial solitons," *Rivista del Nuovo Cimento*, vol. 21, pp. 1–37, 1998.
- [12] E. DelRe, B. Crosignani, M. Tamburrini, M. Segev, M. Mitchell, E. Rafaei, and A. J. Agranat, "One-dimensional steady-state photorefractive spatial solitons in centrosymmetric paraelectric potassium lithium tantalate niobate," *Opt. Lett.*, vol. 23, pp. 421–423, 1998.
- [13] E. DelRe, M. Tamburrini, R. Della Pergola, and A. J. Agranat, "Spontaneous self-trapping of optical beams in metastable paraelectric crystals," *Phys. Rev. Lett.*, vol. 83, pp. 1954–1957, 1999.
- [14] E. DelRe, M. Tamburrini, and A. J. Agranat, "Soliton electro-optic effects in paraelectrics," *Opt. Lett.*, vol. 25, pp. 963–965, 2000.
- [15] E. DelRe, A. Ciattoni, and A. J. Agranat, "Anisotropic charge displacement supporting isolated photorefractive optical needles," *Opt. Lett.*, vol. 26, pp. 908–910, 2001.
- [16] E. DelRe and A. J. Agranat, "Dielectric nonlinearity in photorefractive spatial soliton formation," *Phys. Rev. A, Gen. Phys.*, vol. 65.053 814, pp. 1–5, 2002.
- [17] A. Yariv and P. Yeh, *Optical Waves in Crystals: Propagation & Control of Laser Radiation*. New York: Wiley, 1983, pp. 256–264.
- [18] S. H. Wemple and M. DiDomenico Jr., *Electrooptical and Nonlinear Optical Properties of Crystals*, R. Wolfe, Ed. New York: Academic, 1983, p. 264.
- [19] S. Gatz and J. Herrmann, "Anisotropy, nonlocality, and space-charge field displacement in  $(2 + 1)$ -dimensional self-trapping in biased photorefractive crystals," *Opt. Lett.*, vol. 23, pp. 1176–1178, 1998.

- [20] ———, “Propagation of optical beams and the properties of two-dimensional spatial solitons in media with a local saturable nonlinear refractive index,” *J. Opt. Soc. Amer. B, Opt. Phys.*, vol. 14, pp. 1795–1806, 1997.
- [21] W. Krolikowski, N. Akhmediev, B. Luther-Davies, and M. Cronin-Golomb, “Self-bending photorefractive solitons,” *Phys. Rev. E, Stat. Phys. Plasmas Fluids Relat. Interdiscip. Top.*, vol. 54, pp. 5761–5765, 1996.
- [22] J. Petter, C. Weilna, C. Denz, A. Stepken, and F. Kaiser, “Self-bending of photorefractive solitons,” *Opt. Commun.*, vol. 170, pp. 291–297, 1999.
- [23] M. Saffman and A. A. Zozulya, “Circular solitons do not exist in photorefractive media,” *Opt. Lett.*, vol. 23, pp. 1579–1581, 1998.
- C. Crognale** (M’98), photograph and biography not available at the time of publication.
- L. Rosa**, photograph and biography not available at the time of publication.